J. KSIAM Vol.19, No.1, 47–56, 2015 http://dx.doi.org/10.12941/jksiam.2015.19.047

A MODIFIED CAHN–HILLIARD EQUATION FOR 3D VOLUME RECONSTRUCTION FROM TWO PLANAR CROSS SECTIONS

SEUNGGYU LEE[1], YONGHO CHOI[1], DOYOON LEE[2], HONG-KWON JO[2], SEUNGHYUN LEE[2], SUNGHYUN MYUNG[2], AND JUNSEOK KIM[1,†]

[1]DEPARTMENT OF MATHEMATICS, KOREA UNIVERSITY, SEOUL 136-713, KOREA
[2]SEOUL SCIENCE HIGH SCHOOL, SEOUL 110-530, KOREA

ABSTRACT. In this paper, we present an implicit method for reconstructing a 3D solid model from two 2D cross section images. The proposed method is based on the Cahn–Hilliard model for the image inpainting. Image inpainting is the process of reconstructing lost parts of images based on information from neighboring areas. We treat the empty region between the two cross sections as inpainting region and use two cross sections as neighboring information. We initialize the empty region by the linear interpolation. We perform numerical experiments demonstrating that our proposed method can generate a smooth 3D solid model from two cross section data.

1. INTRODUCTION

Medical imaging, such as computerized tomography (CT), has greatly increased the information available to surgeons and becomes one of the most important diagnostic methods [1]. Medical imaging devices produce three-dimensional medical data in the form of image slices. In such slice images, the distance between consecutive slices is larger than the size of one pixel of medical images [2].

To process medical imaging, there have been proposed many interpolation techniques. Among them, the simplest one is using linear interpolation with gray scale slices [3, 4, 5, 6]. Grevera and Udupa [7] proposed a shape-based interpolation method to multidimensional grey-level images. The basic idea of the method consists of first segmenting the given slice image data into a binary image data, second converting the binary image into a signed distance image data wherein the point value represents its shortest distance, i.e., positive value for points of the object and negative for those outside from the cross-sectional boundary. The first step, called lifting step, transform n-dimensional grey scene to an $(n+1)$-dimensional binary scene. Priorly, the method has been usually applied to binary data. To extend the idea to gray-level images, they used the density distribution of the scene. In the final step, called collapsing step,

Received by the editors December 19 2014; Revised February 17 2015; Accepted in revised form February 23 2015; Published online March 18 2015.

2000 *Mathematics Subject Classification.* 65D18, 68U05.

Key words and phrases. Volume reconstruction, image inpainting, Cahn–Hilliard equation, linear interpolation, finite difference method.

† Corresponding author. Email: cfdkim@korea.ac.kr; Tel: +82 2 3290 3077; Fax: +82 2 929 8562; http://math.korea.ac.kr/∼cfdkim.

$(n+1)$-dimensional binary scene generated by previous processes is inversely transformed to n-dimensional grey scene. This method is considered as both scene- and object-based method. The shape-based interpolation method was also studied in [8].

Guo et al. [1] developed a morphology-based interpolation method by means of a combined operation of weighted dilation and erosion to overcome drawbacks of a shaped-based interpolation method. The significant advantage of the method is that the interpolation could be successful when two given objects are disjointed. It has been considered as the drawback in methods based on mathematical morphology. There are three major steps in its algorithm: (i) make the source and target objects be overlapped on one image, (ii) derive dilation and erosion vectors at contour of source image and (iii) Determine the size of structure and apply dilation or erosion process. However, this method has still heavy computational cost and is not able to handle heavy invaginated objects [9]. Lee and Wang proposed another kinds of morphology-based interpolation method in [10]. Their method gave both reduced computational cost significantly and flexibility of interpolating three-dimensional structure.

Moreover, Lee and Lin [2] proposed a feature-guided shape-based image interpolation scheme which integrates feature line-segments to guide the shape-based method for better shape interpolation. Their proposed method is able to carry out basic image modification such as translation, rotation and scaling when given initial images are similar. Also, the scheme is also valid to dissimilar images.

There are two classification in reconstruction method: explicit and implicit surface methods. The explicit surface method prescribes the surface geometry in an explicit manner. Whereas, the implicit surface method uses a scalar function and present the surface using a zero level set of the function.

In this paper, we propose a fast and accurate implicit numerical method of a partial differential equation based mathematical model for the three-dimensional volume reconstruction from two slice data.

This paper is organized as follows. In Section 2, we describe the governing equations for the image segmentation and the volume reconstruction. Section 3 describes a numerical scheme for the volume reconstruction. In Section 4, we perform some characteristic numerical experiments with synthetic and real medical images for volume reconstruction. Finally, our conclusion is given in Section 5.

2. Reconstruction process

To reconstruct a three-dimensional volume from a set of slice data, we consider the following Cahn–Hilliard equation [11]:

$$\frac{\partial \phi(\mathbf{x},t)}{\partial t} = \Delta \mu(\mathbf{x},t),\ \mathbf{x}\in\Omega,\ 0<t\le T, \tag{2.1}$$

$$\mu(\mathbf{x},t) = F'(\phi(\mathbf{x},t)) - \epsilon^2 \Delta \phi(\mathbf{x},t), \tag{2.2}$$

where $\mathbf{x}=(x,y,z)$ is the three-dimensional coordinate, $\Omega \subset \mathbb{R}^3$ is a domain, $\phi(\mathbf{x},t)$ is a phase-field, which is defined as 1 and -1 in the inside and outside of the reconstructed volume, and $F(\phi)=0.25(1-\phi^2)(1+\phi^2)$. The surface of the volume is represented by the zero level

set of ϕ. Let $\phi_{top}(x, y)$ and $\phi_{bottom}(x, y)$ be the top and the bottom section data on slices S_2 and S_1, respectively (see Fig. 1).

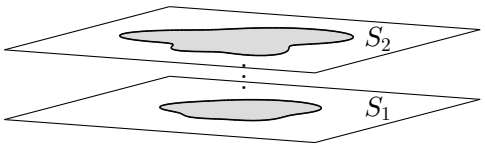

FIGURE 1. Schematic of slice data

The initial condition is the linear interpolation from two slice data:

$$\phi(x, y, \theta z_2 + (1-\theta)z_1) = \theta\phi_{top}(x, y) + (1-\theta)\phi_{bottom}(x, y),\ 0 \le \theta \le 1. \quad (2.3)$$

Dirichlet boundary condition is applied to ϕ and homogeneous Neumann boundary condition is used to μ, i.e., $\mathbf{n} \cdot \nabla\mu = 0$ on $\partial\Omega$. Here, $\mathbf{n}$ is the unit normal vector to the domain boundary $\partial\Omega$. From the boundary condition of μ, there is a constraint condition: $\int_\Omega \phi$ is constant. Equations (3.1) and (3.2) is a gradient flow using an H^{-1} norm from the following total energy functional [12]:

$$\mathcal{E}(\phi) = \int_\Omega \left[F(\phi(\mathbf{x}, t)) + \frac{\epsilon^2}{2}|\nabla\phi(\mathbf{x}, t)|^2 \right] d\mathbf{x}. \quad (2.4)$$

Detailed description of physical, mathematical, and numerical aspects of view can be shown in [14]. We use the idea from the image inpainting problems [15] and volume reconstruction problem [13]. The major difference comparing the previous work in [13] is that we do not use a fidelity term. See [12] to details of a fidelity term.

However, we do not use a fidelity term as used in the previous work [12]. Instead, we use a Dirichlet type boundary condition.

3. NUMERICAL SOLUTION

For the temporal discretization, we use the unconditionally gradient stable Eyre's scheme [16, 17]. We discretize the governing Eqs. (2.1) and (2.2) in three-dimensional space, $\Omega_d = (0, L_x) \times (0, L_y) \times (0, L_z)$. Let $x_i = (i - 0.5)h,\ y_j = (j - 0.5)h,\ z_k = (k - 0.5)h$, $1 \le i \le N_x,\ 1 \le j \le N_y, 1 \le k \le N_z$, where N_x, N_y, and N_z are integers and $h = L_x/N_x = L_y/N_y = L_z/N_z$ is the uniform mesh size. Let ϕ^n_{ijk} be an approximation of $\phi(x_i, y_j, z_k, n\Delta t)$, where $\Delta t = T/N_t$ is the time-step, T is the final time, and N_t is the total number of time-steps.

Then, we have the following discretization:

$$\begin{aligned}\phi_{ijk}^{n+1} &= \phi_{ijk}^{n} + \Delta t \left(\frac{\mu_{i+1,jk}^{n+1} + \mu_{i-1,jk}^{n+1}}{h^2} \right. \\ &\quad \left. + \frac{\mu_{i,j+1,k}^{n+1} + \mu_{i,j-1,k}^{n+1} + \mu_{ij,k+1}^{n+1} + \mu_{ij,k-1}^{n+1} - 6\mu_{ijk}^{n+1}}{h^2} \right), \qquad (3.1) \\ \mu_{ijk}^{n+1} &= (\phi_{ijk}^{n+1})^3 - \phi_{ijk}^{n} - \epsilon^2 \left(\frac{\phi_{i+1,jk}^{n+1} + \phi_{i-1,jk}^{n+1}}{h^2} \right. \\ &\quad \left. + \frac{\phi_{i,j+1,k}^{n+1} + \phi_{i,j-1,k}^{n+1} + \phi_{ij,k+1}^{n+1} + \phi_{ij,k-1}^{n+1} - 6\phi_{ijk}^{n+1}}{h^2} \right). \qquad (3.2)\end{aligned}$$

We solve the discrete system of Eqs. (3.1) and (3.2) by using a Gauss–Seidel iteration. It should be remarked that since we use the Gauss–Seidel iteration there is no restriction on the number of N_z, unlike in the multigrid method which has a better performance in a computational point of view.

Let $\phi_{ijk}^{n+1,m}$ and $\mu_{ijk}^{n+1,m}$ be m-th iterations of the Gauss–Seidel relaxation. Note that $\phi_{ij}^{n+1,m}$ for $i = 1, N_x$, $j = 1, N_y$, and $k = 1, N_k$ are not updated by the Gauss-Seidel relaxation because of its Dirichlet boundary condition. To describe a Gauss–Seidel iteration process, we first define the source term as $(\varphi_{ijk}^{n}, \psi_{ijk}^{n}) = \left(\phi_{ijk}^{n}/\Delta t, -\phi_{ijk}^{n}\right)$. Linearizing $(\phi_{ijk}^{n+1})^3$ at $\phi_{ijk}^{n+1,m}$, we get $(\phi_{ijk}^{n+1})^3 \approx (\phi_{ijk}^{n+1,m})^3 + 3(\phi_{ijk}^{n+1,m})^2(\phi_{ijk}^{n+1} - \phi_{ijk}^{n+1,m})$. Then, we can rewrite Eqs. (3.1) and (3.2) as follows:

$$\begin{aligned}&\frac{\phi_{ijk}^{n+1,m+1}}{\Delta t} + \frac{6\mu_{ijk}^{n+1,m+1}}{h^2} \\ &\quad = \varphi_{ijk}^{n} + \left(\frac{\mu_{i+1,jk}^{n+1,m} + \mu_{i-1,jk}^{n+1,m} + \mu_{i,j+1,k}^{n+1,m} + \mu_{i,j-1,k}^{n+1,m} + \mu_{ij,k+1}^{n+1,m} + \mu_{ij,k-1}^{n+1,m}}{h^2} \right), \qquad (3.3)\end{aligned}$$

and

$$\begin{aligned}&-3\left(\frac{2\epsilon^2}{h^2} + (\phi_{ijk}^{n+1,m})^2 \right) \phi_{ijk}^{n+1,m+1} + \mu_{ijk}^{n+1,m+1} = \psi_{ijk}^{n} - 2(\phi_{ijk}^{n+1,m})^3 \\ &\quad -\epsilon^2 \left(\frac{\phi_{i+1,jk}^{n+1,m} + \phi_{i-1,jk}^{n+1,m} + \phi_{i,j+1,k}^{n+1,m} + \phi_{i,j-1,k}^{n+1,m} + \phi_{ij,k+1}^{n+1,m} + \phi_{ij,k-1}^{n+1,m}}{h^2} \right). \qquad (3.4)\end{aligned}$$

One Gauss–Seidel iteration consists of solving the linear system (3.3) and (3.4) by inversion of 2×2 matrix for each i, j and k. This process will stop when the number of iteration is over 50 since it is practically enough, i.e., more number of iteration does not affect to the result, or ∞-norm of error $||\phi_{ijk}^{n+1,m+1} - \phi_{ijk}^{n+1,m}||_\infty$ is less than a given tolerance, 10^{-5}. We update

values at the top and bottom sections using the following weighted average:

$$\phi_{ij1}^{n+1} = \alpha\phi_{ij1}^{0} + (1-\alpha)(2\phi_{ij2}^{n+1} - \phi_{ij3}^{n+1}), \tag{3.5}$$

$$\phi_{ijN_z}^{n+1} = \alpha\phi_{ijN_z}^{0} + (1-\alpha)(2\phi_{ij,N_z-1}^{n+1} - \phi_{ij,N_z-2}^{n+1}), \tag{3.6}$$

where the weighted average constant $\alpha \in [0,1]$.

We adaptively adjust the temporal step size Δt. If the number of Gauss-Seidel iterations is less than or equal to 3, then we double the size. While the number of iterations is bigger than 3, we divide the size in halves. From this adaptive time method, we can reduce a computational cost in the time interval whose error is small enough or have more accuracy in the time interval whose error is too large.

4. NUMERICAL TESTS

In this section, we perform several numerical experiments to demonstrate the performance of our proposed scheme. Across the interfacial transition region, the concentration field varies from -0.9 to 0.9 over a distance of approximately $2\sqrt{2}\epsilon\,\tanh^{-1}(0.9)$. Therefore, if we want this value to be approximately m grid points, the ϵ value needs to be taken as follows: $\epsilon_m = hm/[2\sqrt{2}\tanh^{-1}(0.9)]$ [18]. To overcome the phenomenon called "spontaneous shrinking", which would make unnatural reconstructed shapes, we consider the diffused initial condition. If the spontaneous shrinking happens, a zero contour shrinks spontaneously while the phase-variable ϕ shifts from its expected values in the bulk phases even though ϕ is conserved globally [19]. Let ϵ_m be the coefficient we want to use, then we give an initial condition as $\phi^0(\mathbf{x}) = \tanh(\mathbf{x}/(\sqrt{2}\epsilon_{2m})$ rather than $\tanh(\mathbf{x}/(\sqrt{2}\epsilon_m)$. Unless otherwise specified, we will stop the numerical computations after 100 time step iterations and parameters ϵ_4, time step $\Delta t = h$, and $N_z = 7$ are used.

4.1. **Energy decreasing.** We first check energy decreasing with time in discrete sense before performing numerical simulations for volume reconstruction. From (2.4), the discrete energy $\mathcal{E}^h(\phi)$ can be defined as follow:

$$\begin{aligned}\mathcal{E}^h(\phi^n) &= \sum_{i=1}^{N_x-1}\sum_{j=1}^{N_y-1}\sum_{k=1}^{N_z-1}\frac{\epsilon^2 h^3}{2}\left[(\phi_{i+1,jk}-\phi_{ijk})^2 + (\phi_{i,j+1,k}-\phi_{ijk})^2 + (\phi_{ij,k+1}-\phi_{ijk})^2\right] \\ &\quad + \sum_{i=1}^{N_x}\sum_{j=1}^{N_y}\sum_{k=1}^{N_z} F(\phi_{ijk}^n)h^3.\end{aligned} \tag{4.1}$$

Here, the initial conditions are given as two disks with radii 0.15:

$$\phi_{ij1}^0 = \tanh\left(\left[0.15 - \sqrt{(x_i-0.3)^2 + (y_j-0.5)^2}\right] \Big/ (\sqrt{2}\epsilon)\right),$$

and

$$\phi_{ijN_z}^0 = \tanh\left(\left[0.15 - \sqrt{(x_i-0.3)^2 + (y_j-0.5)^2}\right] \Big/ (\sqrt{2}\epsilon)\right).$$

Figure 2 represents the graph of $\mathcal{E}^h(\phi^n)$ versus time. The result shows that the discrete energy functional decreasing holds.

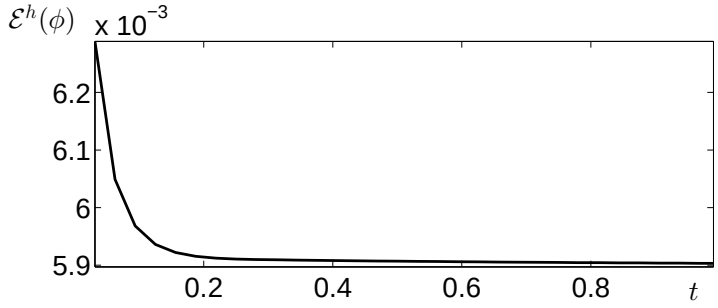

FIGURE 2. Graph of $\mathcal{E}^h(\phi^n)$ versus time.

4.2. **Effect of weight average constant α.** We perform numerical simulations to compare the effect of weight average constant α in Eqs. (3.5) and (3.6). We choose the slices S_1 and S_2 as disks with radii 0.3 and 0.2:

$$\phi^0_{ij1} = \tanh\left(\left[0.3 - \sqrt{(x_i - 0.4)^2 + (y_j - 0.5)^2}\right] \Big/ (\sqrt{2}\epsilon)\right)$$

and

$$\phi^0_{ijN_z} = \tanh\left(\left[0.2 - \sqrt{(x_i - 0.4)^2 + (y_j - 0.5)^2}\right] \Big/ (\sqrt{2}\epsilon)\right).$$

Figure (3) shows the reconstructed isosurface with (a) $\alpha = 0.1$ and (b) $\alpha = 0.5$. We can clearly see that the case with $\alpha = 0.5$ has much better performance than the other. Consequently, we set $\alpha = 0.5$ unless otherwise specified in later simulations.

(a) $\alpha = 0.1$ (b) $\alpha = 0.5$

FIGURE 3. Reconstructed isosurface with (a) $\alpha = 0.1$ and (b) $\alpha = 0.5$.

4.3. **Oblique cylinder.** We observe the 3D reconstruction with two elliptic slices in this section. Let S_1 and S_2 be as follows:

$$\phi^0_{ij1} = \tanh\left(\left[0.2 - \sqrt{c(x_i - 0.4)^2 + 0.5(y_j - 0.5)^2}\right] \Big/ (\sqrt{2}\epsilon)\right)$$

and

$$\phi^0_{ijN_z} = \tanh\left(\left[0.2 - \sqrt{c(x_i - 0.6)^2 + 0.5(y_j - 0.5)^2}\right] \Big/ (\sqrt{2}\epsilon)\right),$$

where $c = \sin(\tan^{-1}(5(N_z - 1)h))$. The expected reconstruction result is an oblique cylinder whose cross section is a circle like $x^2 + y^2 = 0.2^2$ since the initial slices are given as elliptic shapes. To see a relation of this initial condition and expected 3-dimensional structure, Fig. (4) can be a helpful schematic.

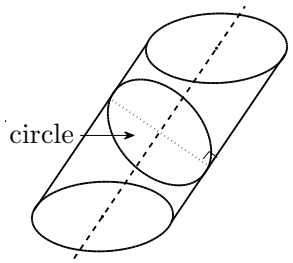

FIGURE 4. Schematic of an oblique cylinder.

Figure (5) shows the temporal evolution of the reconstructed isosurfaces. The temporal step size $\Delta t = 0.1h$ and the final iteration number is 1000. The final isosurface structure is well-matched to our expectation from a little dented initial isosurface.

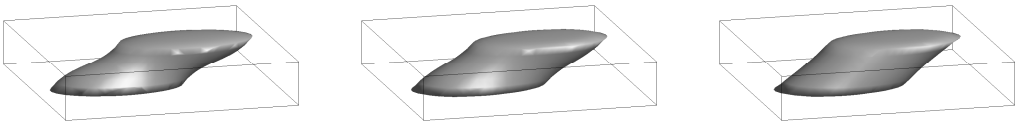

(a) Initial (b) 100 iteration (c) 1000 iterations

FIGURE 5. Temporal evolution of the reconstructed isosurfaces.

4.4. **Various initial data.** We consider four different configurations. The slices S_1 and S_2 are given as

$$
\begin{aligned}
\text{(a) Bottom} \quad &: \quad \phi^0_{ijN_z} = \tanh\left(\left[0.3 - \sqrt{(x_i-0.5)^2 + 0.5(y_j-0.5)^2}\right] \Big/ (\sqrt{2}\epsilon)\right), \\
\text{Top} \quad &: \quad \phi^0_{ij1} = \tanh\left(\left[0.3 - \sqrt{0.5(x_i-0.5)^2 + (y_j-0.5)^2}\right] \Big/ (\sqrt{2}\epsilon)\right), \\
\text{(b) Bottom} \quad &: \quad \phi^0_{ijN_z} = \tanh\left(\left[0.2 - \sqrt{(x_i-0.5)^2 + (y_j-0.5)^2}\right] \Big/ (\sqrt{2}\epsilon)\right), \\
\text{Top} \quad &: \quad \phi^0_{ij1} = \frac{1}{2}\Big[\Big(\tanh\Big([x-0.15] \Big/ (\sqrt{2}\epsilon)\Big) - \tanh\Big([x-0.85] \Big/ (\sqrt{2}\epsilon)\Big)\Big) \\
&\qquad \times \Big(\tanh\Big([y-0.15] \Big/ (\sqrt{2}\epsilon)\Big) - \tanh\Big([y-0.85] \Big/ (\sqrt{2}\epsilon)\Big)\Big) - 1\Big], \\
\text{(c) Bottom} \quad &: \quad \phi^0_{ijN_z} = \tanh\left(\left[0.3 - \sqrt{(x_i-0.5)^2 + (y_j-0.5)^2}\right] \Big/ (\sqrt{2}\epsilon)\right), \\
\text{Top} \quad &: \quad \phi^0_{ij1} = 1 + \tanh\left(\left[0.15 - \sqrt{(x_i-0.3)^2 + (y_j-0.3)^2}\right] \Big/ (\sqrt{2}\epsilon)\right) \\
&\qquad + \tanh\left(\left[0.15 - \sqrt{(x_i-0.7)^2 + (y_j-0.7)^2}\right] \Big/ (\sqrt{2}\epsilon)\right), \\
\text{(d) Bottom} \quad &: \quad \phi^0_{ijN_z} = \tanh\left(\left[0.3 - \sqrt{(x_i-0.5)^2 + (y_j-0.5)^2}\right] \Big/ (\sqrt{2}\epsilon)\right), \\
\text{Top} \quad &: \quad \phi^0_{ij1} = 2 + \tanh\left(\left[0.1 - \sqrt{(x_i-0.3)^2 + (y_j-0.3)^2}\right] \Big/ (\sqrt{2}\epsilon)\right) \\
&\qquad + \tanh\left(\left[0.1 - \sqrt{(x_i-0.7)^2 + (y_j-0.5)^2}\right] \Big/ (\sqrt{2}\epsilon)\right) \\
&\qquad + \tanh\left(\left[0.1 - \sqrt{(x_i-0.3)^2 + (y_j-0.7)^2}\right] \Big/ (\sqrt{2}\epsilon)\right).
\end{aligned}
$$

In Fig. (6), left columns represent contours of S_1 and S_2. Right columns represent isosurfaces reconstructed from respective contours. It is demonstrated that our proposed method has a good performance of reconstruction with various initial slice data.

5. CONCLUSIONS

In this paper, we presented an implicit method for reconstructing a 3D solid model from two 2D cross section images. Our proposed model was based on the Cahn–Hilliard equation used in the image inpainting field. Reconstructing lost parts of images was proceeded based on information from neighboring areas. As inpainting region, the empty region between the two cross sections was treated and two cross sections were used as neighboring information. Linear interpolation was used when initializing the empty region. We performed numerical experiments demonstrating that our proposed method can generate a smooth 3D solid model

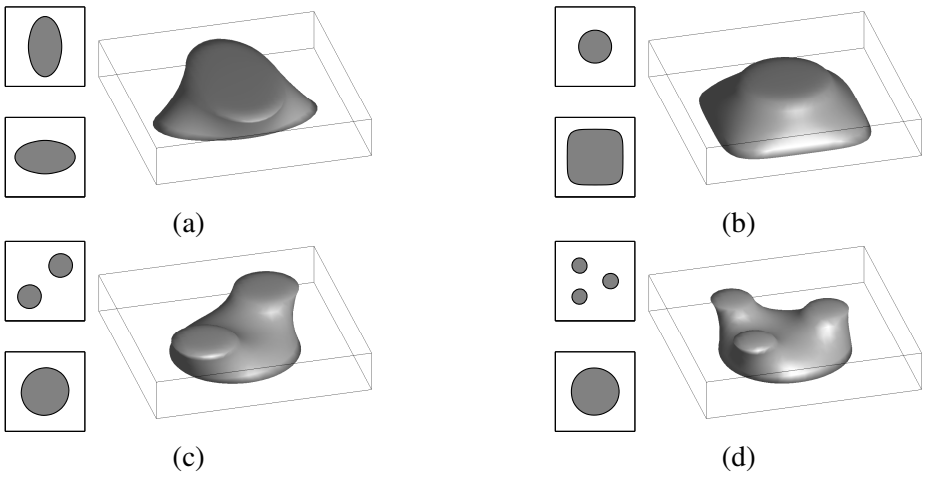

FIGURE 6. Left columns represent contours of S_1 and S_2. Right columns represent isosurfaces reconstructed from respective contours.

from two cross section data. Different constant for weighted average was considered for better performance. Various cases such as oblique cylinder, perpendicular ellipses, circle and square and branches showed a smooth 3D solid structures. As a future work, we will investigate the extension of the proposed algorithm to multi-slice cross sections.

ACKNOWLEDGMENT

The corresponding author (J.S. Kim) was supported by the National Research Foundation of Korea(NRF) grant funded by the Korea government(MSIP) (NRF-2014R1A2A2A01003683). This work was supported by Seoul Science High School R&E program in 2014

REFERENCES

[1] J.F. Guo, Y.L. Cai, and Y.P. Wang, *Morphology-based interpolation for 3D medical image reconstruction*, Comput. Med. Imaging Graph., **19** (1995), 267–279.

[2] T.Y. Lee and C.H. Lin, *Feature-guided shape-based image interpolation*, IEEE Trans. Med. Imaging, **21** (2002), 1479–1489.

[3] H. Fuchs, Z. M. Kedem, and S. P. Uselton, *Optimal surface reconstruction from planar contours*, Commun. ACM, **20** (1977), 693–702.

[4] G. Herman and C. Coin, *The use of 3D computer display in the study of disk disease*, J. Comput. Assist. Tomogr., **4**(4) (1980), 564–567.

[5] C.C. Liang, C.T. Chen, and W.C. Lin, *Intensity interpolation for reconstructing 3-D medical images from serial cross-sections*, Engineering in Medicine and Biology Society, Proceedings of the Annual International Conference of the IEEE, (1988), 1389–1390.

[6] C.C. Liang, C.T. Chen, and W.C. Lin, *Intensity interpolation for branching in reconstructing three-dimensional objects from serial cross-sections*, Medical Imaging V: Image Processing. International Society for Optics and Photonics, (1991), 456–467.

[7] G.J. Grevera and J.K. Udupa, *Shape-based interpolation of multidimensional grey-level images*, IEEE Trans. Med. Imaging, **15** (1996), 881–892.
[8] G.T. Herman, J. Zheng, and C.A. Bucholtz, *Shape-based interpolation*, IEEE Comput. Graphics Apllicat., **12** (1992), 69–79.
[9] Y.H. Liu, Y.N. Sun, C.W. Mao, and C.J. Lin, *Edge-shrinking interpolation for medical images*, Comput. Vis. Graphics Image Processing, **21**(2) (1997), 91–101.
[10] T.Y. Lee and W.H. Wang, *Morphology-based three-dimensional interpolation*, IEEE Trans. Med. Imag. **19** (2000), 711–721.
[11] J.W. Cahn, *On Spinodal Decomposition*, Acta Metall. Mater., **9**(9) (1961), 795–801.
[12] A. Bertozzi, S. Esedoglu and A. Gillette, *Inpainting of binary images using the Cahn–Hilliard equation*, IEEE Trans. Image. Proc., **16** (2007), 285–291.
[13] Y. Li, J. Shin, Y. Choi and J. Kim, *Three-dimensional volume reconstruction from slice data using phase-field models*, Comput. Vis. Image Und. DOI:10.1016/j.cviu.2015.02.001, 2015.
[14] D. Lee, J-Y. Huh, D. Jeong, J. Shin, A. Yun, and J. Kim, *Physical, mathematical, and numerical derivations of the Cahn–Hilliard equation*, Comput. Mater. Sci., **81** (2014), 216–225.
[15] D. Jeong, Y. Li, H.G. Lee and J. Kim, *Fast and automatic inpainting of binary images using a phase-field model*, J. KSIAM, **13** (2009), 225–236.
[16] D. Eyre, *An unconditionally stable one-step scheme for gradient systems*, unpulished article, http://www.math.utah.edu/∼eyre/research/methods/stable.ps, (1998).
[17] S. Lee, C. Lee, H.G. Lee, and J. Kim, *Comparison of different numerical schemes for the Cahn–Hilliard equation*, J. KSIAM, **17**(3) (2013), 197–207.
[18] J.J. Eggleston, G.B. McFadden, and P.W. Voorhees, *Phase-field model for highly anisotropic interfacial energy*, Phys. D, **150** (2001), 91–103.
[19] P. Yue, C. Zhou and J.J. Feng, *Spontaneous shrinkage of drops and mass conservation in phase-field simulations*, J. Comput. Phys., **223** (2007), 1–9.